

# *Distributed energy storage control for dynamic load impact mitigation*

Article

Accepted Version

Creative Commons: Attribution 4.0 (CC-BY)

Open access

Zangs, M. J., Adams, P. B. E., Yunusov, T. ORCID: <https://orcid.org/0000-0003-2318-3009>, Holderbaum, W. ORCID: <https://orcid.org/0000-0002-1677-9624> and Potter, B. A. (2016) Distributed energy storage control for dynamic load impact mitigation. *Energies*, 9 (8). 647. ISSN 1996-1073 doi: 10.3390/en9080647 Available at <https://centaur.reading.ac.uk/66549/>

It is advisable to refer to the publisher's version if you intend to cite from the work. See [Guidance on citing](#).

Published version at: <http://www.mdpi.com/1996-1073/9/8/647>

To link to this article DOI: <http://dx.doi.org/10.3390/en9080647>

Publisher: MDPI Publishing, Basel

All outputs in CentAUR are protected by Intellectual Property Rights law, including copyright law. Copyright and IPR is retained by the creators or other copyright holders. Terms and conditions for use of this material are defined in the [End User Agreement](#).

[www.reading.ac.uk/centaur](http://www.reading.ac.uk/centaur)

**CentAUR**

Central Archive at the University of Reading

Reading's research outputs online

Article

# Distributed Energy Storage Control for Dynamic Load Impact Mitigation

Maximilian J. Zangs<sup>1,†</sup>, Peter B. E. Adams<sup>1,†</sup>, Dr Timur Yunusov<sup>1</sup>, Dr William Holderbaum<sup>1\*</sup> and Dr Ben A. Potter<sup>1</sup>

<sup>1</sup> School of Systems Engineering, University of Reading, Whiteknights Campus, RG6 6AY, Reading, United Kingdom

<sup>†</sup> These authors contributed equally to this work.

\* Author to whom correspondence should be addressed; w.holderbaum@reading.ac.uk, Tel: +44 1183 786086, Fax: +44 1189 751994

Version January 30, 2016 submitted to *Energies*. Typeset by L<sup>A</sup>T<sub>E</sub>X using class file *mdpi.cls*

---

1     **Abstract:** The future uptake of Electric Vehicles (EV) in low-voltage distribution networks  
2     can cause increased voltage violations and thermal overloading of network assets, especially  
3     in networks with limited headroom at times of minimum or peak demand. To address the  
4     problem, this paper proposes a distributed battery energy storage solution, controlled using  
5     an Additive Increase Multiplicative Decrease (AIMD) algorithm. The proposed AIMD+  
6     algorithm uses local voltage measurements and a reference voltage threshold to determine  
7     the Additive Increase parameter and to control the charging and discharging of the battery.  
8     The voltage threshold used is dependent on the network topology and is calculated using  
9     power flow analysis, with peak demand equally allocated between loads. Simulations were  
10    performed on the IEEE European test case and a number of real UK suburban networks,  
11    using European demand data and a realistic electric vehicle travel model. The performance  
12    of the standard AIMD algorithm with fixed voltage threshold and the proposed AIMD+  
13    algorithm with reference voltage profile are compared. Results show that, compared to the  
14    standard AIMD case, the proposed AIMD+ algorithm improves the voltage profile, reduces  
15    thermal overloads and ensures fairer battery utilisation.

16    **Keywords:** Battery storage; Distributed control; Electric vehicles; AIMD; Voltage control;  
17    Smart grid

---

## 18 **1. Introduction**

19 The adoption of Electric Vehicles (EV) is seen as a potential solution to the decarbonisation of future  
20 transport network, offsetting emissions from conventional internal combustion engine vehicles. Current  
21 rate of EV uptake is anticipated to increase with improved driving range, reduced cost of purchase and  
22 greater emphasis on leading an environmentally friendly lifestyle [1]. It is predicted that by 2030, there will  
23 be three million Plug-in Hybrid Electric Vehicles and EVs sold in Great Britain and Northern Ireland [2],  
24 and it is expected that by 2020 every tenth car in the United Kingdom will be electrically powered [3].  
25 It is anticipated that the majority of PHEV/EV will be charged at home, which puts additional stress on  
26 the existing local low voltage distribution network, which must provide the increased demand in energy  
27 [4,5]. Uncontrolled charging of multiple PHEV/EV raises the daily peak power demand, which leads  
28 to: increased transmission line losses, higher voltage drops, equipment overload, damage, and failure  
29 [6–9]. Accommodating the increased demand and mitigation of such failures is a major area of research  
30 interest, with the focus mainly placed on the coordinating and support of home-charging.

31 Demand Side Management (DSM) strategies, that aim to alleviate the impacts of PHEV/EV  
32 home-charging, are a favoured solution. Mohsenian-Rad *et.al.* in [10] developed a distributed DSM  
33 algorithm that implicitly controls the operation of loads, based on game theory and the network operator's  
34 ability to dynamically adjust energy prices. Focusing on financial incentive driven DSM strategies, in  
35 [11], a time-of-use (TOU) tariff and real-time load management strategy was proposed, where disruptive  
36 charging is avoided by allocating higher prices to times of peak demand. In addition, Distributed  
37 Generation (DG) has also been included with the optimisation of PHEV/EV charging using financial  
38 incentives [12].

39 Research focused on grid support has been driven by the need to deliver long term savings and to avoid  
40 the immediate costs and disruption of network reinforcements and upgrades. This research proposes the  
41 implementation of alternative solutions to support the adoption of low carbon technologies, such as  
42 Electric Vehicles and Heat pumps. To reduce the occurrence increased peak demands, Mohsenian-Rad  
43 *et.al.* developed an approach of direct interaction between grid and consumer to achieve valley-filling,  
44 by means of dynamic game theory [10]. In [13], a MAS was used to manage flexible loads for the  
45 minimisation of cost in a dynamic game. The use of aggregators has been proposed to allow the  
46 participation of a number of small providers to participate in network support, such as grid frequency  
47 response [14–16].

48 Research focused on grid support has been driven by the need to deliver long term savings and to avoid  
49 the immediate costs and disruption of network reinforcements and upgrades. This research proposes the  
50 implementation of alternative solutions to support the adoption of low carbon technologies, such as  
51 Electric Vehicles and Heat pumps. To reduce the occurrence increased peak demands, Mohsenian-Rad  
52 *et.al.* developed an approach of direct interaction between grid and consumer to achieve valley-filling,  
53 by means of dynamic game theory [10]. In [13], a MAS was used to manage flexible loads for the  
54 minimisation of cost in a dynamic game. The use of aggregators has been proposed to allow the  
55 participation of a number of small providers to participate in network support, such as grid frequency  
56 response [14–16].

57 In this paper, a similar approach to support electricity distribution feeders is proposed, where  
58 dedicated energy storage units mitigate the effects of disruptive loads, such as the high uptake of  
59 Electric Vehicles. An Additive Increase Multiplicative Decrease (AIMD) type algorithm is proposed for  
60 control of the battery energy storage devices. AIMD algorithms were originally applied to congestion  
61 management in communications networks using the TCP protocol[17], to maximise utilisation while  
62 ensuring a fair allocation of data throughput amongst a number of competing users. AIMD-type  
63 algorithms have been applied to power sharing scenarios in low voltage distribution networks, where  
64 the limited resource is the availability of power from the substation's transformer. An AIMD-type  
65 algorithm was first proposed for EV Charging by Stüdli *et.al.* [18], requiring a one-way communications  
66 infrastructure to broadcast a 'capacity event', this was further developed to include vehicle-to-grid  
67 applications with reactive power support [19,20]. The proposed battery control algorithm builds upon  
68 work by Mareels *et.al.* [21], to include bidirectional power flow and the use of a reference voltage profile  
69 derived from network models.

70 The remainder of this paper is organised as follows: Section 2 outlines the EV, network and storage  
71 models used in the research. Additionally it explains the assumptions that accommodate and validate  
72 these models. Section 3 elaborates on the proposed AIMD control algorithm (AIMD+). Next, Section  
73 4 details the implementation and scenarios used for particular test cases that. For later comparison, this  
74 section also outlines a set of comparison metrics. Section 5 presents and discusses the results, followed  
75 by the conclusion in Section 6.

## 76 2. System Modelling

77 In this section, the underlying assumptions to validate the research are addressed. Next, a model  
78 to describe Electric Vehicle charging behaviour is explained. This is followed by a model of the  
79 battery energy storage. Finally, the network models used to simulate the power distribution networks  
80 are explained.

### 81 2.1. Assumptions

82 For this work several underlying assumption were made to generate the models:

- 83 1. The uptake of EVs is assumed to increase and hence have a significant impact on the normal  
84 operation of the low voltage distribution network. This assumption is based on a well established  
85 prediction that the majority of EV charging will take place at home [22].
- 86 2. The transition from internal combustion engine powered vehicles to EVs is assumed to not impact  
87 the users' driving behaviour. Similar to [23], this assumption allows the utilisation of recent  
88 vehicle mobility data [24] to generate leaving, driving and arriving probabilities, from which the  
89 EV charging demand can be determined.
- 90 3. The transition to low carbon technologies will likely increase the variability and flexibility of  
91 demand and so support devices, such as battery energy storage, are anticipated to play a more  
92 important role. Hence, alongside a high uptake of Electric Vehicles, an increased adoption of  
93 distributed energy storage devices is assumed.

- 94 4. It is assumed that energy storage solutions, or more specifically battery storage solutions, start the  
 95 simulations at 50% SOC and are not 100% efficient at storing and releasing electrical energy, as in  
 96 [25]. Additionally, its utilisation will degrade the energy storage capability and performance over  
 97 time as shown in [26]. Therefore the requirements for fair storage usage is of primary importance.
- 98 5. It is assumed that the load profiles provided by the IEEE Power and Energy Society (PES) are  
 99 sufficient as base load profiles for all simulations.

## 100 2.2. Electric Vehicle Charging Behaviour

101 From publicly available car mobility data [23,24] an empirical model was developed to capture the  
 102 underlying driving behaviour. The raw data,  $n_r(t)$ , represents the probabilities of starting a trip during a  
 103 15 minutes period of a weekday. Three continuous normal distribution functions, each defined as:

$$\hat{n}_x(t) = \beta_x \frac{1}{\sigma_x \sqrt{2\pi}} \exp \left[ -\frac{(t/24 - \mu_x)^2}{2\sigma_x^2} \right] \text{ where } t = [0, 24] \quad (1)$$

104 were used to represent vehicles leaving in the morning,  $\hat{n}_m(t)$ , lunch time,  $\hat{n}_l(t)$ , and in the evening,  
 105  $\hat{n}_e(t)$ . The aggregate probability of these three functions was optimised using a Generalised Reduced  
 106 Gradient (GRG) algorithm to fit the original data. In order to represent a symmetric commuting  
 107 behaviour, i.e. vehicles departing in the morning return during the evening, an equality amongst the  
 108 three probabilities was defined as follows:

$$0 = \int_0^{24} [\hat{n}_m(t) + \hat{n}_l(t) - \hat{n}_e(t)] dt \quad (2)$$

109 The resulting parameters from the GRG fitting of the three distribution functions are tabulated in  
 110 Table 1. Additionally, the resulting departure probabilities, as well as the reference data  $n_r(t)$  are shown  
 111 in Figure 1.

**Table 1.** Parameters for normal distributions

Equation $\hat{n}_x(t)$	$\mu_x$ (mean)	$\sigma_x$ (Std. Dev.)	$\beta_x$ (weight)
$\hat{n}_m(t)$	0.3049	0.0488	0.00206
$\hat{n}_l(t)$	0.4666	0.0829	0.00314
$\hat{n}_e(t)$	0.7042	0.0970	0.00521

112 Statistical data capturing the probability distribution of a trip being of a certain distance was also  
 113 extracted from the dataset. This was done for both the weekdays  $w_{wd}(d)$  and weekends  $w_{we}(d)$ . The  
 114 Weibull function was chosen to be fitted against the extracted probability distributions, and is defined as:

$$\hat{w}_x(d) := \begin{cases} \frac{k_x}{\gamma_x} \left( \frac{d}{\gamma_x} \right)^{k_x-1} \exp \left[ -\left( \frac{d}{\gamma_x} \right)^{k_x} \right] & \text{if } d \geq 0 \\ 0 & \text{if } d < 0 \end{cases} \quad (3)$$

115 Performing the curve fitting using the GRG optimisation algorithm, a weekday trip distances  
 116 distribution,  $\hat{w}_{wd}(d)$ , and a weekend trip distribution,  $\hat{w}_{we}(d)$  could be estimated. The computed

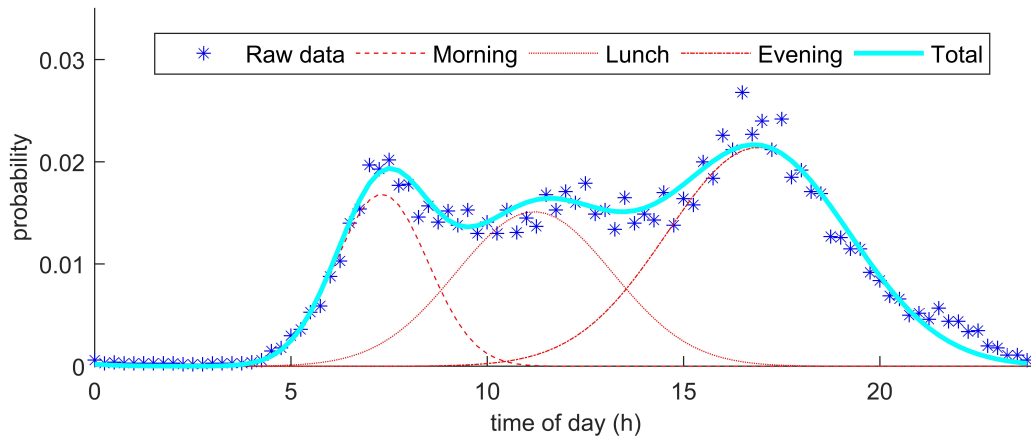


**Figure 1.** The probability of starting a trip at a particular time during a weekday, extrapolated into three normal distributions (RMS error: 9.482%).

117 function parameters for these two estimated distribution functions are tabulated in Table 2. Their  
 118 resulting probability distributions are plotted for comparison against the real data in Figure 2.

119

**Table 2.** Parameters for Weibull distributions

Equation $\hat{w}_x(d)$	$\gamma_x$ (scale)	$k_x$ (shape)
$\hat{w}_{wd}(t)$	15.462	0.6182
$\hat{w}_{we}(t)$	38.406	0.4653

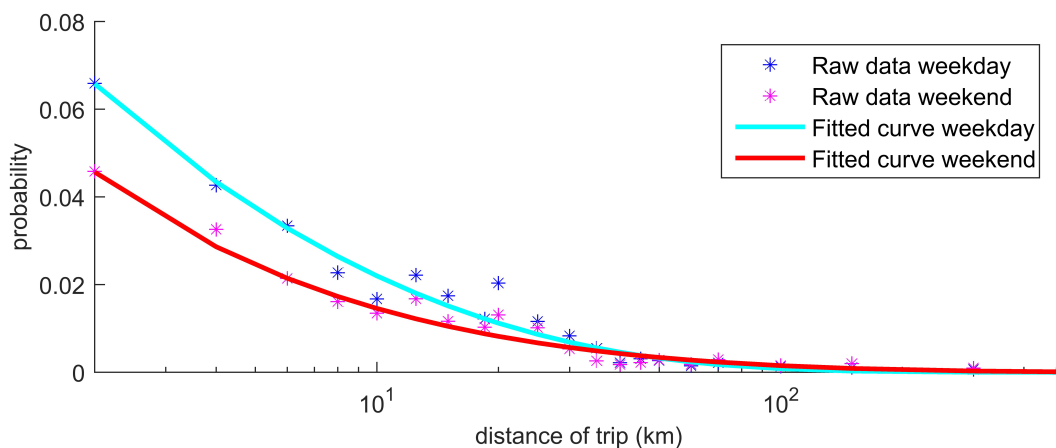


**Figure 2.** The probability of a trip being of a particular distance during a weekday, extrapolated into a Weibull distribution (RMS error: 3.791%).

120 In addition to these probabilities, an average driving speed of 56kmh (35mph) and an average driving  
 121 energy efficiency of 0.1305 kWh/kmh (0.21 kWh/mph) are taken from [27]. Using the predicted driving  
 122 distance and average driving speed with the driving energy efficiency, it is possible to estimate an EV's  
 123 energy demand upon arrival. Starting to charge from this arrival time until the energy demand has been  
 124 met allowed to generate an estimated charging profile of a single EV. To do so, a maximum charging  
 125 power of 5kW and an immediate disconnection of the EV upon charge completion was assumed.

126 Generating several of those charging profiles and aggregating them produces an estimated charging  
 127 demand for an entire fleet of EVs. To provide an example, charge demand profiles for 50 EVs were  
 128 generated, aggregated and plotted in Figure 3. This plot shows the expected magnitude and variability  
 129 in energy demand that is required to charge several EVs at consumers' homes based upon the vehicles'  
 130 daily useage. This data, was used to feed additional demand into the network models, which are outlined  
 131 in the next section.

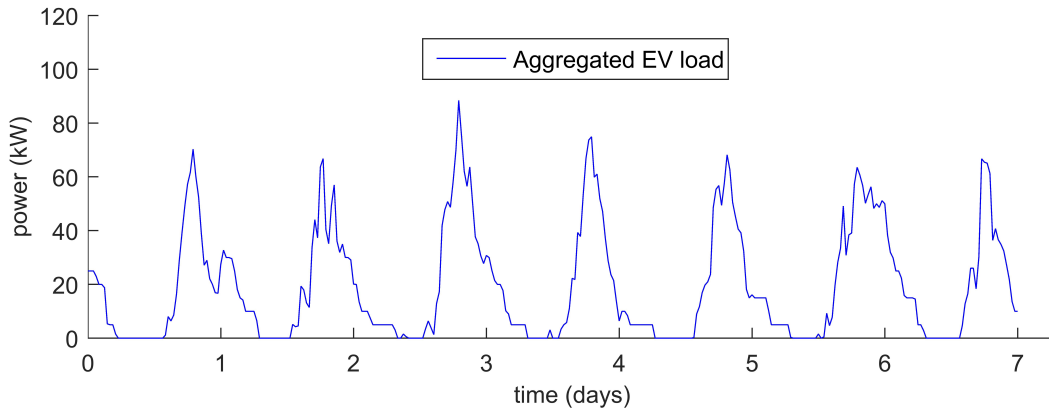


**Figure 3.** Excerpt from the aggregated 50 EVs, rated at 5kW, charging powers that were each generated from the empirical models.

### 132 2.3. Battery Modelling

133 For this work, a well established model that has been used in previous publications by this research  
 134 group was used [25,28]. Typically, an ideal battery changes its State of Charge (SOC) depending on the  
 135 power that flows into it,  $P_{bat}$ . When analysing the battery system at a regular sampling period  $\tau$ , then the  
 136 energy transferred into the system can be described as  $P_{bat}\tau$ . Optimally, the change in SOC,  $\delta_{SOC}$ , can  
 137 be described as follows:

$$\delta_{SOC}(t) = P_{bat}(t)\tau = \text{SOC}(t) - \text{SOC}(t - \tau) \quad (4)$$

138 Adding standby and conversion losses, respectively  $\eta_s$  and  $\hat{\eta}_c$ , the evolution in SOC can be  
 139 summarised as follows:

$$\text{SOC}(t) = (1 - \eta_s)\text{SOC}(t - \tau) + \hat{\eta}_c\delta_{SOC}(t) \quad (5)$$

140 Here, the conversion losses in the power electronics are reflected as an asymmetric efficiency, which  
 141 depends on the direction of the flow of energy. This is done by charging the battery at a lower rate  
 142 when consuming energy, and discharging it quicker when exporting energy. Mathematically, this can be  
 143 represented as:

$$\hat{\eta}_c = \begin{cases} \eta_s & \text{if } \delta_{SOC}(t) \geq 0 \\ \frac{1}{\eta_s} & \text{if } \delta_{SOC}(t) < 0 \end{cases} \quad (6)$$

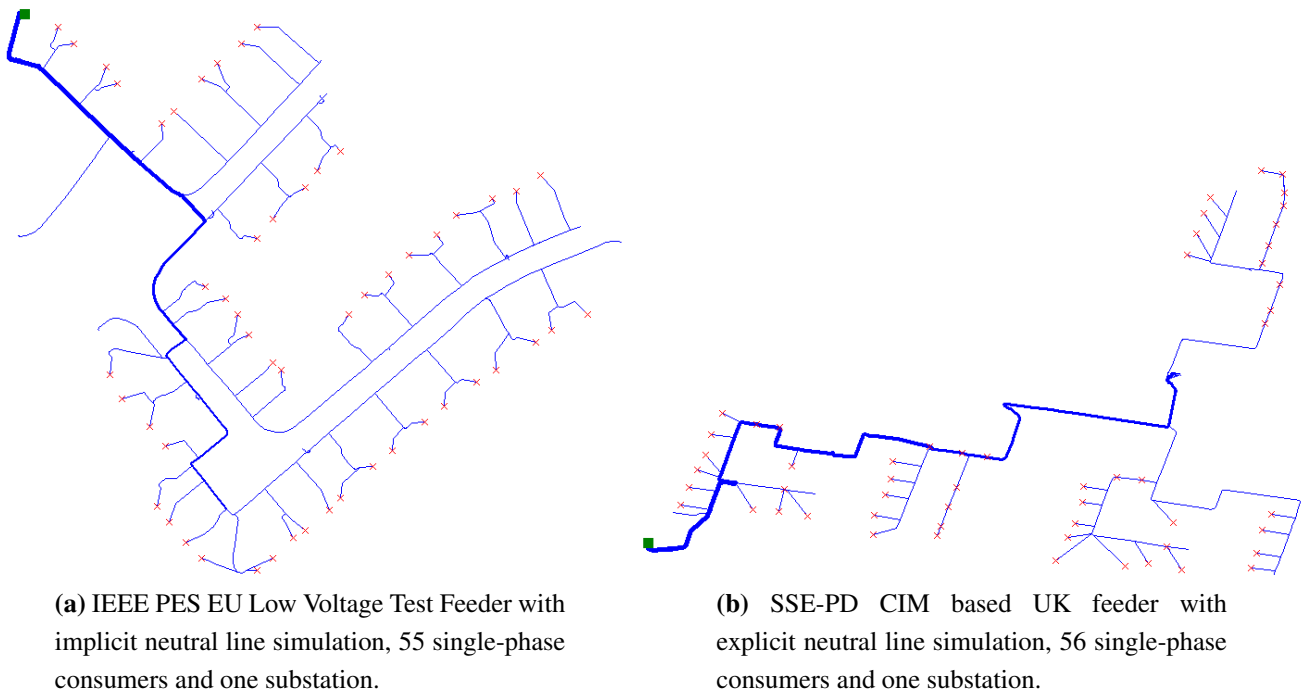
144 In addition, both the SOC and  $P_{bat}$  are restricted due to the devices energy storage capabilities and  
 145 maximum charge and discharge rate. These limitations are captured in Equation 7 and Equation 8,  
 146 respectively.

$$\text{SOC}_{min} < \text{SOC}(t) < \text{SOC}_{max} \quad (7)$$

$$|P_{bat}(t)| \leq P_{max} \quad (8)$$

#### 147 2.4. Network Models

148 To simulate the low-voltage energy distribution grid, the Open Distribution System Simulator  
 149 (OpenDSS) developed by the Electronic Power Research Institute (EPRI) was used. It requires element  
 150 based network models, including line, load and transformer information, and generates realistic power  
 151 flow results.



(a) IEEE PES EU Low Voltage Test Feeder with implicit neutral line simulation, 55 single-phase consumers and one substation.

(b) SSE-PD CIM based UK feeder with explicit neutral line simulation, 56 single-phase consumers and one substation.

**Figure 4.** Sample OpenDSS power flow plots of the used power networks. Consumers are indicated as red crosses and 11/0.416kV substations are marked with a green square.

152 The IEEE-PES's European Low Voltage Test Feeder was used for this work [29], and a set of detailed  
 153 UK feeder models, provided by Scottish and Southern Energy Power Distribution (SSE-PD) were used,  
 154 too. The SSE-PD circuit models were provided as Common Information Models (CIM) during the  
 155 collaboration on the New Thames Valley Vision Project Project (NTVV) [30]. An example of the  
 156 IEEE-PES EU LV Test feeder and a UK feeder provided by SSE-PD are shown in Figure 4a and Figure  
 157 4b, respectively. The model derived EV data and IEEE PES consumer demand profiles were used in  
 158 all simulations. The resultant demand profiles represent the total daily electricity demand of households  
 159 with EVs. These profiles were sampled at  $\tau = 1$  minute. The openDSS simulation environment is control  
 160 using MATLAB. This was achieved through OpenDSS's Common Object Model (COM) interface and  
 161 is accessible using Microsoft's ActiveX server bridge.

### 162 3. Storage Control

163 In this section, the control of the energy storage system is explained. Firstly, the Additive Increase  
164 Multiplicative Decrease (AIMD) algorithm is presented, then an improved voltage threshold is explained.

#### 165 3.1. Additive Increase Multiplicative Decrease

166 The proposed distributed battery storage control is shown in Algorithm 1. The parameter  $\alpha$  denotes  
167 the size of the power's Additive Increase step and  $\beta$  denotes the size of the Multiplicative Decrease  
168 step. The constants  $V_{max}$  and  $V_{thr}$  are used to regulate the total demand. More specifically, when the  
169 total demand is too high, the local voltages will drop below  $V_{thr}$  and the batteries will start to reduce  
170 their charging power or start discharging, in order to reduce total demand on the feeder.  $V_{max}$  is set to  
171 the nominal voltage of the substation transformer, 240V, and  $V_{thr}$  is set to some fraction of  $V_{max}$ . The  
172 variable  $V(t)$  is the local voltage and  $P_{max}$  denotes the maximum charging/discharging power of the  
173 battery.

---

#### Algorithm 1 Compute Battery Power

---

```

1:  $R(t) = (V(t) - V_{thr}) / (V_{max} - V_{thr})$            ▷ Defines the rate for the current voltage reading
2: if  $V(t) \geq V_{thr}$  then                               ▷ Given the voltage levels are nominal...
3:   if  $SOC < 0.9$  then                                   ▷ ...and the battery is not fully charged...
4:      $P(t) = P(t - \tau) + \alpha P_{max} R(t)$              ▷ ...increase the charging power
5:   else                                                 ▷ If the battery has fully charged...
6:      $P(t) = 0$                                          ▷ ...shut off
7:   end if
8:   if  $P(t) < 0$  then                                   ▷ If the battery has been discharging...
9:      $P(t) = \beta P(t - \tau)$                            ▷ ...quickly reduce the injected power
10:  end if
11: else                                                 ▷ If voltage levels are not nominal...
12:   if  $SOC > 0.1$  then                                   ▷ ...and battery is charged sufficiently...
13:      $P(t) = P(t - \tau) + \alpha P_{max} R(t)$              ▷ ...increase injected power
14:   else                                                 ▷ If the battery is not sufficiently charged...
15:      $P(t) = 0$                                          ▷ ...shut off
16:   end if
17:   if  $P(t) > 0$  then                                   ▷ If the battery has been charging...
18:      $P(t) = \beta P(t - \tau)$                            ▷ ...quickly reduce the charging power
19:   end if
20: end if
21:  $P(t) = \text{signum}(P(t)) \times \min\{|P(t)|, P_{max}\}$  ▷ Limit the power to battery specifications, i.e.  $\pm 2\text{kW}$ 

```

---

174 The algorithm is characterised by two states of operation. During periods of low demand, the local  
175 voltage is higher than the threshold voltage and so the battery is set to charge. If the  $V(t) < V_{thr}$  while  
176 charging, the rate,  $R(t)$ , becomes negative and the charging power of the battery is reduced. When

177 demand is high and  $V(t) < V_{thr}$  for a sustained period, then the battery begins to discharge. In contrast,  
 178 if the  $V(t) > V_{thr}$  while discharging, the rate,  $R(t)$ , becomes positive and the discharging power of the  
 179 battery is reduced. The charging and discharging power of the batteries is incremented in proportion  
 180 to the available headroom on the network, inferred from local voltage measurement  $V(t)$ . Yet with  
 181  $V(t) \rightarrow V_{thr}$ , the power increment for each battery is reduced to avoid sudden overload of the substation  
 182 transformer.

### 183 3.2. Reference Voltage Profile

184 When using a fixed voltage threshold, the difference in location and load of each customer results in  
 185 the over utilisation of batteries located at the feeder end. Similar to Papaioannou *et.al.* [31], a reference  
 186 voltage profile is proposed, which is produced by performing a power flow analysis of the network, under  
 187 maximum demand. An example of a fixed threshold and reference voltage profile is shown in Figure 5.

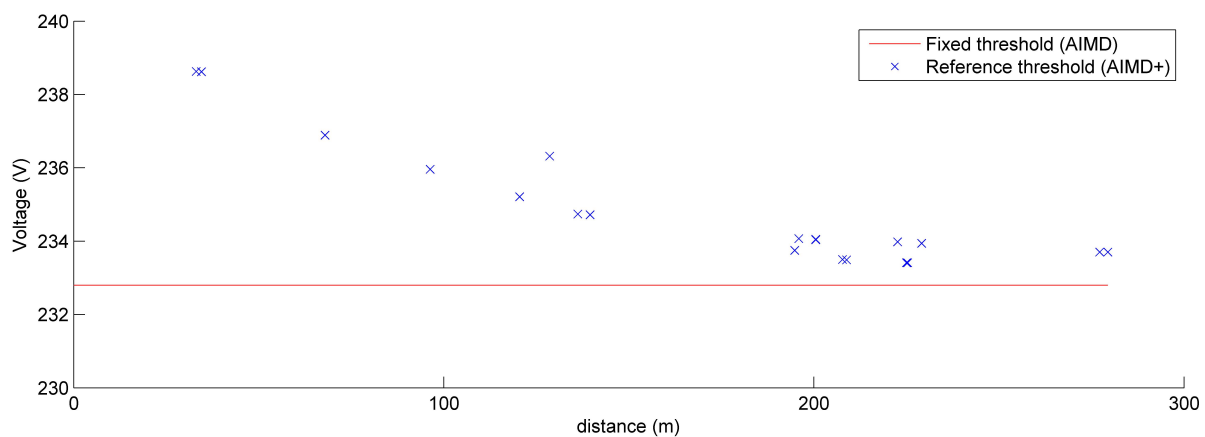


**Figure 5.** A plot showing the difference between the fixed voltage threshold (AIMD) and the reference voltage profile (AIMD+)

188 In the enhanced AIMD algorithm (AIMD+), consumers located at the head of the feeder are allocated  
 189 a higher voltage threshold, while those towards the end of the feeder have similar voltage thresholds to  
 190 that of the fixed threshold. This replicates the expected voltage drop along the length of the feeder and  
 191 so results in a fairer utilisation of battery storage units, that are located at those distances. The voltage  
 192 threshold is set so as to limit maximum voltage drop to 3% at the end of the feeder.

## 193 4. Scenarios and Comparison Metrics

194 In this section, several scenarios are explained that were used to test the performance of the battery  
 195 control algorithm. Following that is a definition of three comparison metrics. These metrics quantify the  
 196 improvements caused by the different algorithms in comparison to the worst case scenario.

#### 197 4.1. Test Cases and Scenarios

198 In simulations the Electric Vehicles plug-in on arrival and charge at rate of 5kW until fully charged.  
199 The battery energy storage devices have a capacity of 7kWh with a maximum power rating of 2kW. Four  
200 test cases were defined with different levels EV and storage uptakes as follows:

- 201 **A** A baseline scenario, where only historic household demand is used.
- 202 **B** A worst case scenario, in which Electric Vehicle uptake is 100% and no battery energy storage is  
203 used.
- 204 **C** An AIMD scenario, in which Electric Vehicle uptake is 100% and each household has a battery  
205 energy storage device. Here, each battery was controlled using the AIMD algorithm using a fixed  
206 voltage threshold.
- 207 **D** An AIMD+ scenario, in which Electric Vehicle uptake is 100% and each household has a battery  
208 energy storage device. Here, each battery was controlled using the AIMD+ algorithm using the  
209 reference voltage profile.

210 A storage uptake of 100% was adopted to represent the worst case scenario. In addition to the four  
211 defined scenarios, a full set of simulations was performed with EV and storage uptake combinations of  
212 0% to 100% in steps of 10%.

#### 213 4.2. Performance Metric Definition

214 To obtain comparable performance metrics, three parameters are defined. These parameters capture  
215 the improvements in voltage violation mitigation, line overload reduction and fairness of battery usage.  
216 The excerpt performance metrics were calculated based on simulations from the IEEE EU test case for  
217 reproducibility .

##### 218 4.2.1. Parameter for voltage improvement

219 The first parameter,  $\zeta^*$ , calculates the magnitude of the voltage level improvement by comparing  
220 two voltage frequency distributions. More specifically, it finds the difference between these probability  
221 distributions and computes a weighted sum. Here, the weighting,  $\delta^*(v)$ , emphasises the voltage level  
222 improvements that deviate more from the nominal substation voltage  $V_{ss}$ . If the resulting weighted  
223 sum is negative, then the obtained voltage frequency distribution has improved in comparison to the  
224 associated worst case scenario. In contrast, a positive number would indicate a worse outcome. The  
225 performance metric is defined in Equation 9.

$$\zeta_{\mathbf{C}}^* := \sum_{v=V_{min}}^{V_{max}} \delta^*(v) [P_{\mathbf{B}}(v) - P_{\mathbf{C}}(v)] \quad (9)$$

226 Here,  $V_{min}$  is the lowest recorded voltage and  $V_{max}$  is the highest recorded voltage.  $P_{\mathbf{B}}(v)$  is the  
227 voltage probability distribution of the worst case scenario (case **B**), and  $P_{\mathbf{C}}(v)$  is the voltage probability

228 distributions of case **C** (i.e. the case with maximum EV and AIMD storage uptake). Cases **B** and **D**  
 229 would therefore be compared by parameter  $\zeta_{\mathbf{D}}^*$ .

230 The aforementioned factor,  $\delta^*(v)$ , scales down the summation in Equation 9 for voltages within the  
 231 nominal operating band, as no voltage violations take place. Voltage violations are scaled up to increase  
 232 their impact on the summation. This scaling was produced using a linear function, symmetric about  $V_{ss}$ ,  
 233 that is defined as:

$$\delta^*(v) := \begin{cases} \frac{V_{ss}-v}{V_{ss}-V_{low}} & \text{if } v \leq V_{ss} \\ \frac{v-V_{ss}}{V_{high}-V_{ss}} & \text{otherwise} \end{cases} \quad (10)$$

234 where,  $V_{low}$  and  $V_{high}$  are defined as the lower and upper limits of the nominal operation voltage  
 235 band, respectively. In general, the proposed voltage comparison parameter,  $\zeta^*$ , shows an improvement  
 236 in voltage distribution when it is negative, whereas a positive value implies a voltage distribution with  
 237 more voltage violations.

#### 238 4.2.2. Parameter for line overload reduction

239 Similar to measuring the voltage level improvements, the line utilisation probability distributions  
 240 between the storage and worst case scenarios were compared. This follows a similar equation described  
 241 in Equation 9, but using a different scaling factor:

$$\zeta_{\mathbf{C}}^{**} := \sum_{c=0}^{C_{max}} \delta^{**}(c) [P_{\mathbf{C}}(c) - P_{\mathbf{B}}(c)] \quad (11)$$

242 Here,  $C_{max}$  is the highest line utilisation.  $P_{\mathbf{B}}(c)$  and  $P_{\mathbf{C}}(c)$  are the line utilisation probability  
 243 distributions for case **B** and **C**, respectively, and  $\delta^{**}(c)$  is the associated scaling factor. Since the  
 244 relationship between line current and ohmic losses is quadratic, this scaling factor is defined as an  
 245 exponential function that amplifies the impact of line currents beyond the line's nominal rating.

$$\delta^{**}(c) = \begin{cases} \left(\frac{c}{1-C_{min}}\right)^2 & \text{if } c \geq C_{min} \\ 0 & \text{otherwise} \end{cases} \quad (12)$$

246 The modifier  $C_{min}$  defines from where the scaling should start and has been set to 0.5 for this work as  
 247 only line utilisation above 0.5 p.u. was considered. Therefore, a reduction in line overloads would give  
 248 a negative  $\zeta^{**}$ , whereas a positive value implies a higher line utilisation.

#### 249 4.2.3. Parameter for improvement of battery cycling

250 The final metric,  $\zeta^{***}$ , gives an indication of the inequality of battery cycling across all battery units.  
 251 It does this by computing the ratio between the peak and mean battery cycling. This Peak-to-Average  
 252 Ratio (PAR) is defined in the following equation.

$$\zeta_{\mathbf{C}}^{***} := \frac{\max |C_{\mathbf{C}}|}{B^{-1} \sum_{b=1}^B |c_{\mathbf{C}}^b|} \quad (13)$$

253 Here,  $B$  is the number of batteries and  $c_C^b$  is the total cycling of battery  $b$  during scenario **C**.  $C_C$  is a  
 254 vector of  $\mathbb{R}_{\geq 0}^B$ , that contains all batteries' cycling values, i.e.  $c_C^b \in C_C$ . Equally, the battery cycling for  
 255 scenario **D** would be captured by  $\zeta_D^{***}$ . In the unlikely event of an equal cycling of all batteries,  $\zeta^{***}$  will  
 256 have a value of one. Yet as batteries are operated differently, the value of  $\zeta^{***}$  is likely to be greater than  
 257 one. Therefore, a resulting PAR closer to one implies a more equal and therefore fairer utilisation of the  
 258 deployed batteries.

## 259 5. Results and Discussion

260 In this section, the results are outlined that were generated from all simulations. In each of the three  
 261 subsections, the performances of the AIMD and AIMD+ algorithm are compared against another. To  
 262 do so, the performance metrics outlined in Section 4.2 are used. In each subsection, results from the  
 263 four test cases defined as **A**, **B**, **C** and **D** in Section 4.1 are explained first, then the results from the full  
 264 analysis over the large range of EV and battery storage uptake is presented. In the end, these results are  
 265 put into context and discussed.

### 266 5.1. Voltage Violation Analysis

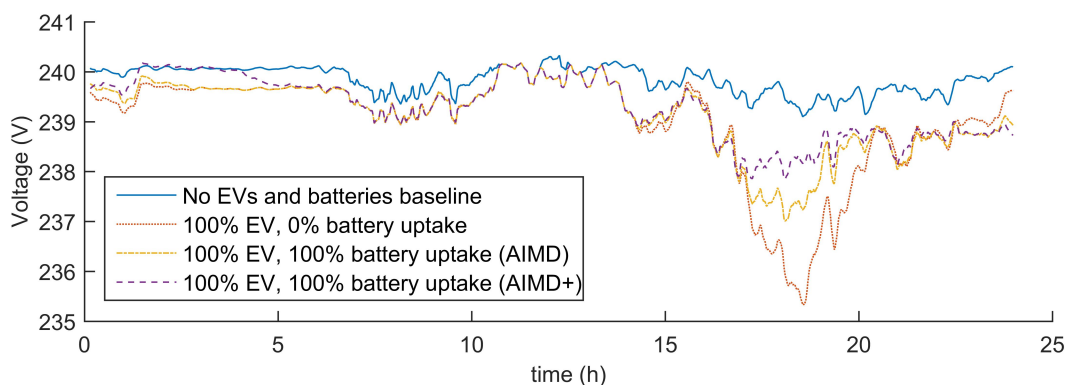


**Figure 6.** Recorded voltage profile at the first consumer's bus over the period of one with a certain uptake in EV and battery storage devices using a moving average over a window of 5 minutes. Here, case **A** is blue, case **B** is red, case **C** is yellow, and case **D** is violet.

267 The results were compared based on their performance at improving the voltage profile of the feeder,  
 268 by increasing the minimum voltage recorded at each bus. Each load's bus voltage was recorded, from  
 269 which a sample voltage profile, Figure 6, was extracted, where the bus voltage fluctuation over time  
 270 becomes apparent. Here, the introduction of EVs has significantly lowered the line-to-neutral voltage.  
 271 Adding energy storage devices has raised the voltage levels during times of peak demand, as can be seen  
 272 between 17:00 - 21:00, where the AIMD+ algorithm has elevated voltages further than AIMD scenario.  
 273 To obtain a better understanding of the level of improvement, the voltage frequency distribution for the  
 274 entire feeder was generated and plotted in a histogram in Figure 7.

275 In this histogram, the voltage probability distribution for all four cases were normalised and plotted  
 276 against another. Here, the previously seen drop in voltages by introducing EVs is recorded as a shift  
 277 in the voltage distribution. This voltage drop is impacted by the introduction of the storage solutions,

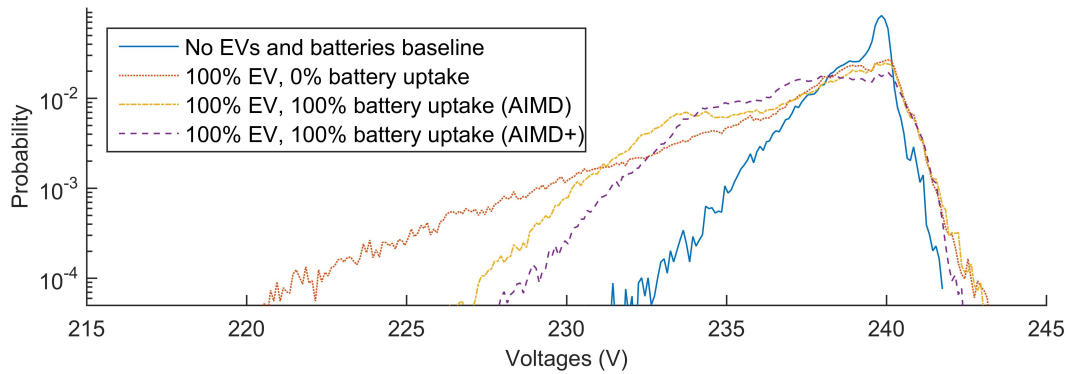


**Figure 7.** Voltage probability distribution of all loads' buses for certain uptakes of EV and battery storage devices. Here, case **A** is blue, case **B** is red, case **C** is yellow, and case **D** is violet with  $\zeta_C^* = -0.0128$  and  $\zeta_D^* = -0.0362$ .

278 since the probability distribution is shifted towards higher voltage bands. For the IEEE PES test case,  
 279 the AIMD+ controlled batteries outperform the AIMD devices as the resulting  $\zeta_C^*$  is greater than  $\zeta_D^*$ .

280 To gain a full understanding of the performance of the AIMD and AIMD+ algorithms, a full sweep  
 281 of EV and storage uptake combinations was simulated on all available power distribution networks. The  
 282 resulting parameters were averaged and plotted in Figure 8.

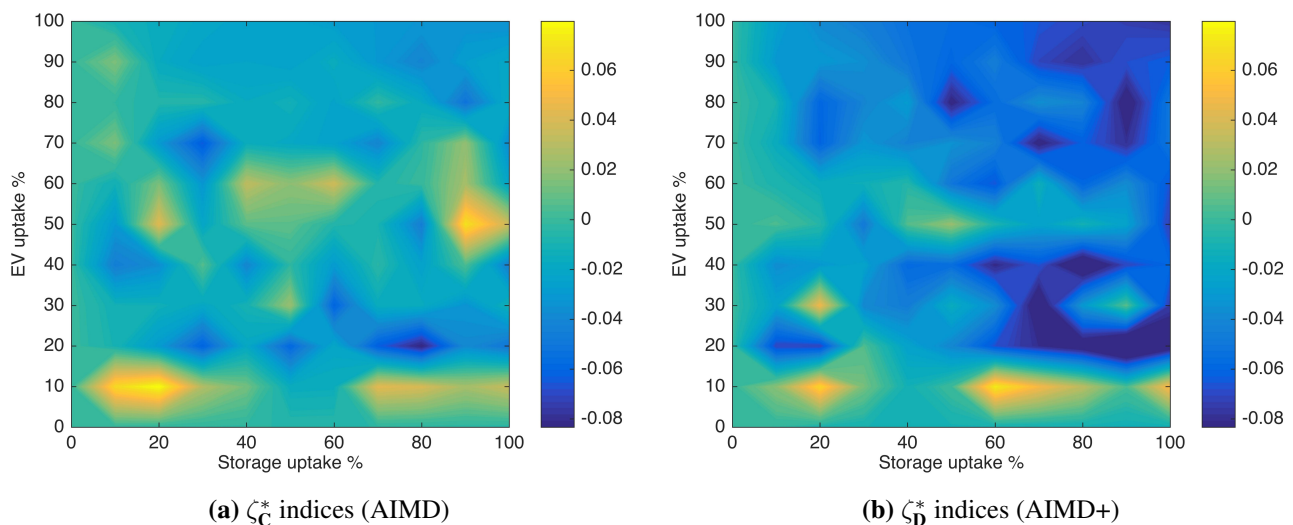


**Figure 8.** Comparison of voltage improvement indices (i.e.  $\zeta^*$ ) for AIMD (Fig. 8a) and AIMD+ (Fig. 8b).

283 These figures show that the AIMD+ control algorithm reduces voltage variation as the uptake in  
 284 storage and EVs increases. The AIMD algorithm does not perform as effectively since more  $\zeta_C^*$  values  
 285 are positive and larger than their corresponding  $\zeta_D^*$  value. This becomes more apparent when removing  
 286 the EV uptake axis and averaging all  $\zeta_C^*$  and  $\zeta_D^*$  values for a their common storage uptake. The resulting  
 287 averaged metrics are plotted in Figure 9.

288 In this last figure the it can be seen how an increase in battery uptake impacts the improvement of  
 289 voltage levels. In fact, both compared algorithms improved the bus voltage distributions, yet the AIMD+  
 290 algorithm noticeably outperformed the AIMD algorithm. This is the case as for every uptake  $\zeta_C^* > \zeta_D^*$ .

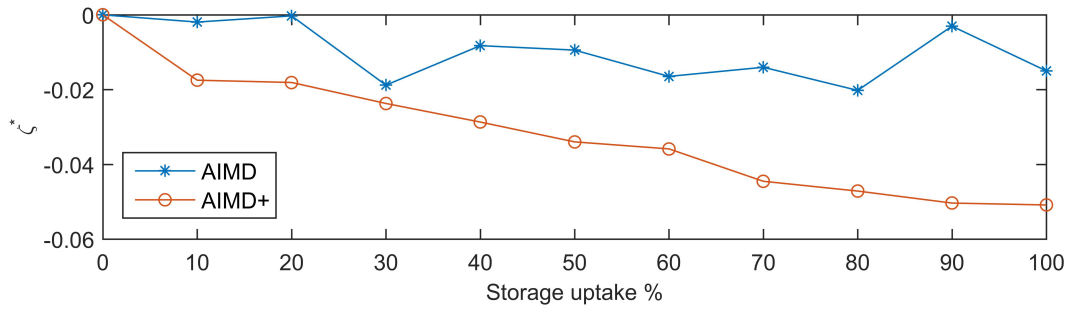


**Figure 9.** Average  $\zeta_C^*$  (AIMD) and  $\zeta_D^*$  (AIMD+) values recorded against the corresponding storage uptake.

## 291 5.2. Line Overload Analysis

292 Similar to the voltage improvement analysis, a frequency distribution of the line utilisation was  
 293 generated. Figure 10 is shows a probability distribution of the per unit current in all lines, for each of  
 294 the four scenarios. The corresponding  $\zeta_C^{**}$  and  $\zeta_D^{**}$  values for the AIMD and AIMD+ storage deployment  
 295 have also been included in the figure's caption.

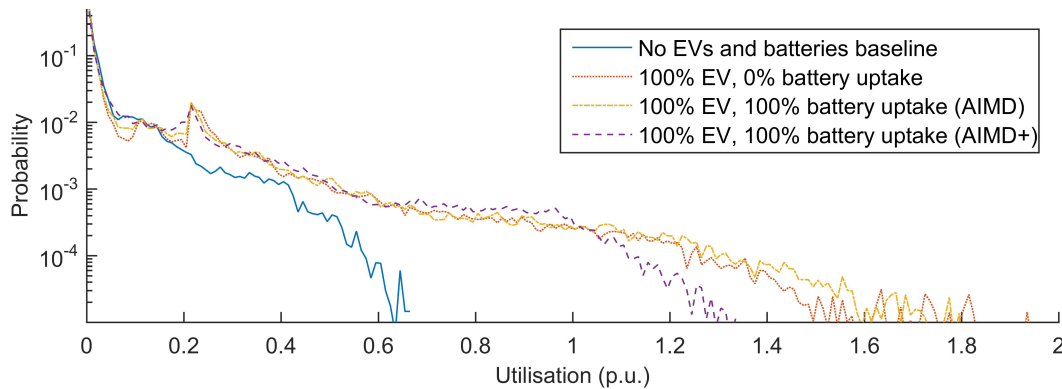


**Figure 10.** Line utilisation probability distribution of all lines in the simulated feeder for certain uptakes of EV and battery storage devices. Here, case **A** is blue, case **B** is red, case **C** is yellow, and case **D** is violet with  $\zeta_C^{**} = 0.174$  and  $\zeta_D^{**} = -0.364$ .

296 Here, the AIMD+ controlled storage devices show a reduction in line overloads. This improvement  
 297 is noticeable through the compressed width of the probability distribution and negative  $\zeta_D^{**}$  value. In  
 298 contrast, the AIMD controlled storage devices do not fully utilise the line capacity as effectively, which  
 299 leads to a positive value of  $\zeta_C^{**}$ . To evaluate the line utilisation improvement across all simulations, the  
 300 full range of EV and storage uptake was evaluated. The resulting plots are shown in Figure 11.

301 In these figures, it can be seen how the performance metrics change as EV and storage uptake  
 302 increases. For the AIMD controlled batteries the resulting  $\zeta_C^{**}$  values are distributed around zero, whereas  
 303 the AIMD+ algorithm achieved mostly negative values of  $\zeta_D^{**}$ . These negative values confirm the higher  
 304 utilisation of line capacity. This becomes more noticeable for scenarios where very low EV uptake is  
 305 combined with very large storage uptake. Here, AIMD controlled storage devices commence their initial  
 306 charge simultaneously, which causes a number of line overloads. The AIMD+ algorithm increases the  
 307 charging gradually, preventing these line overloads from occurring.

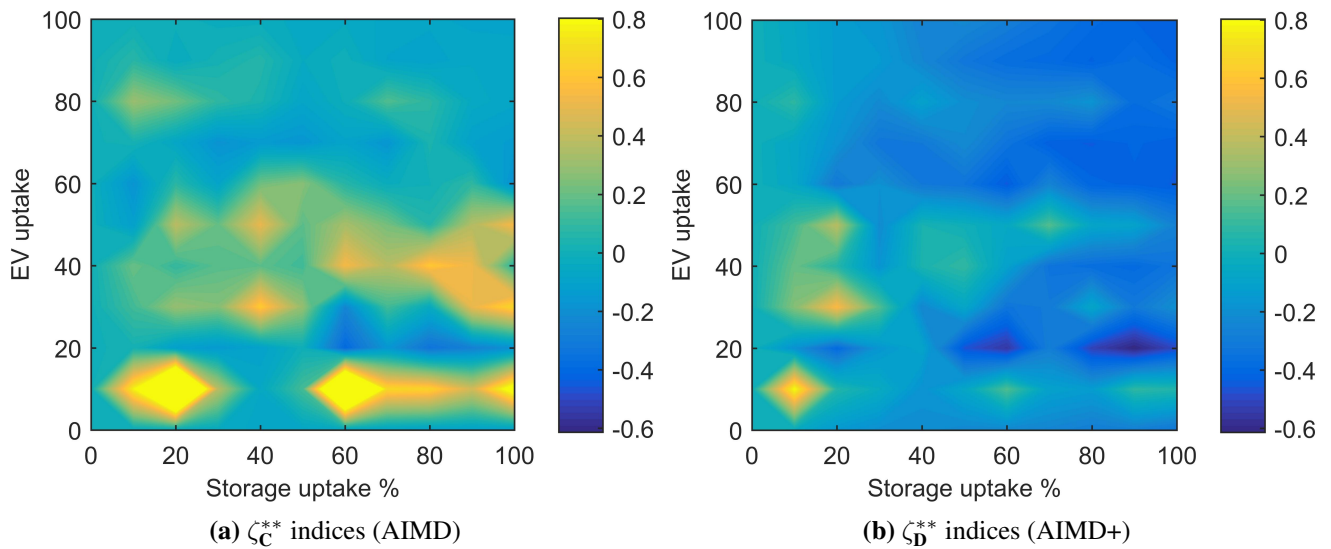


**Figure 11.** Comparison of line utilisation improvement indices for AIMD (Fig. 11a) and AIMD+ (Fig. 11b).

308 Averaging the  $\zeta_C^{**}$  and  $\zeta_D^{**}$  values over all EV uptakes gives an clearer indication of performance, as  
 309 this is now the only variable in the performance analysis. The result is plotted in Figure 12. Here, the  
 310 hypothesis that AIMD controlled energy storage devices do not improve line utilisation is confirmed. In  
 311 contrast, the AIMD+ controlled devices succeed at reducing line overloads. This is also demonstrated by  
 312 the values of  $\zeta_C^{**}$ , which remains positive yet close to zero, whereas  $\zeta_D^{**}$  decreases with increasing uptake  
 313 of battery storage devices.

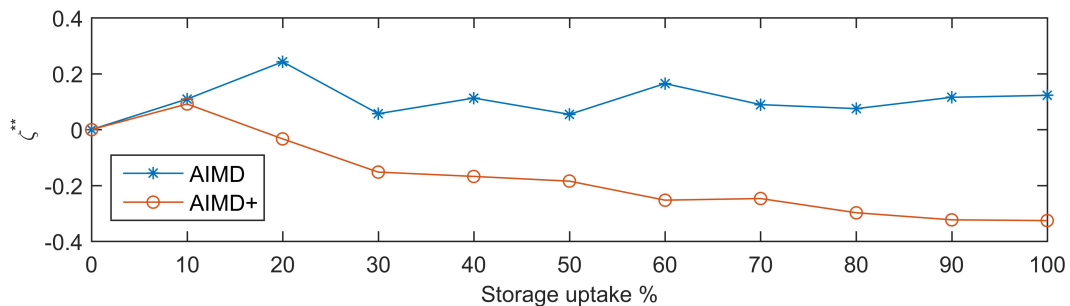


**Figure 12.** Average  $\zeta_C^{**}$  (AIMD) and  $\zeta_D^{**}$  (AIMD+) values recorded against the corresponding storage uptake.

314 Whereas the deployment of energy storage has often been seen as a possible solution to defer network  
 315 reinforcements, the presented results show that this is not the case. In fact, the importance of choosing  
 316 an appropriate control algorithm outweighs the availability of the energy storage itself. This becomes  
 317 particularly apparent when energy storage devices need to recharge their injected energy for times of  
 318 peak demand. For the AIMD case, this recharging is not controlled sufficiently, which leads to higher  
 319 line currents. The proposed AIMD+ algorithm was not as susceptible to this kind of behaviour as it is  
 320 designed to take battery location into account. This immunity and the well controlled power injection  
 321 causes very little to no additional strain on the network's equipment, yet allows the deployed storage  
 322 devices to provide voltage support.

323 *5.3. Battery Utilisation Analysis*

324 In this part of the analysis, the batteries' fairness of usage was evaluated. The battery power profiles  
 325 were recorded and an excerpt has been plotted in Figure 13. These power profiles are arranged by  
 326 distance from the substation.

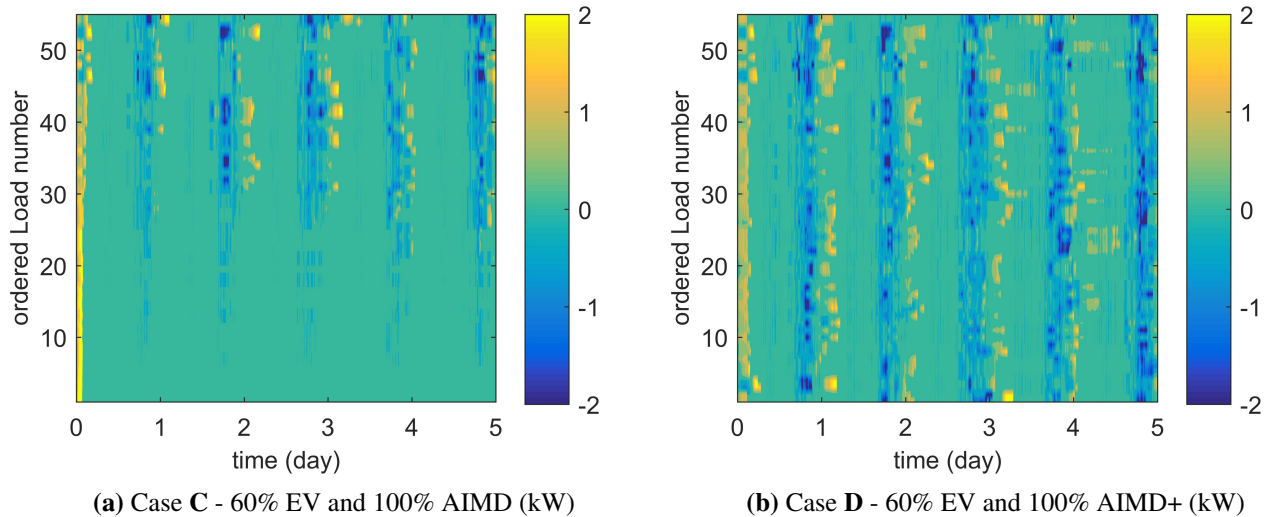


**Figure 13.** Battery power profiles of each load's battery storage device over four days for AIMD (Fig. 13a) and AIMD+ (Fig. 13b).

327 In this figure, it can be seen that only half of the deployed storage devices were active in case C  
 328 (AIMD control), whereas nearly all devices are utilised in case D (AIMD+ control). From the recorded  
 329 battery SOC profiles, the net cycling of each battery was computed and divided by the duration of the  
 330 simulation, giving an average daily cycling value. This is plotted for each load in Figure 14a. The  
 331 corresponding statistical analysis is presented in Figure 14b.

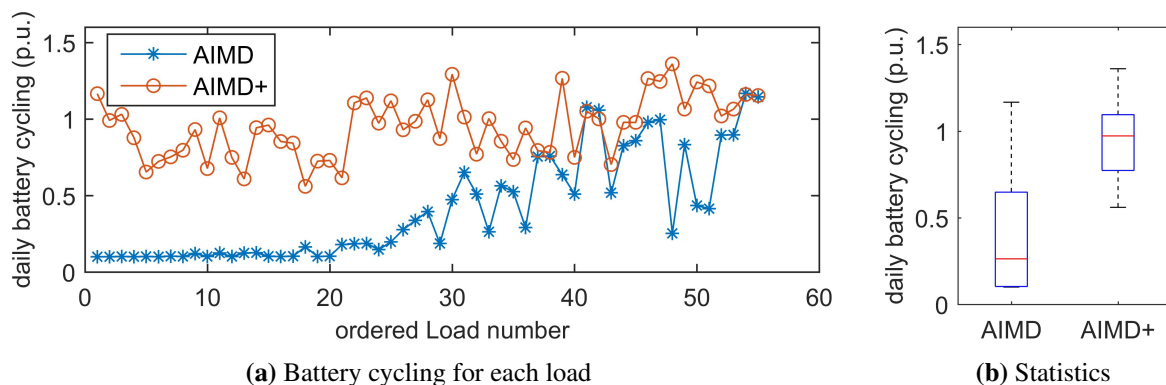


**Figure 14.** Each load's battery cycling compared for 60% EV and 100% AIMD and AIMD+ uptake (Fig. 14a) and in a statistical context (Fig. 14b). Here,  $\zeta_C^{***} = 3.51$  and  $\zeta_D^{***} = 1.61$

332 These two plots show the under-usage of AIMD controlled batteries as well as the imbalance in  
 333 battery usage under AIMD and AIMD+ control. In fact, under AIMD control, 20 out of 55 batteries

334 experience a cycling of less than 10% per day whereas the remaining devices are utilised more fully.  
 335 This discrepancy causes the  $\zeta_C^{***}$  value to be noticeably larger than  $\zeta_D^{***}$ . A more detailed comparison  
 336 was performed by plotting the Peak-to-Average Ratios from the full range of EV and storage uptake  
 337 scenarios and plotted in Figure 15.

338

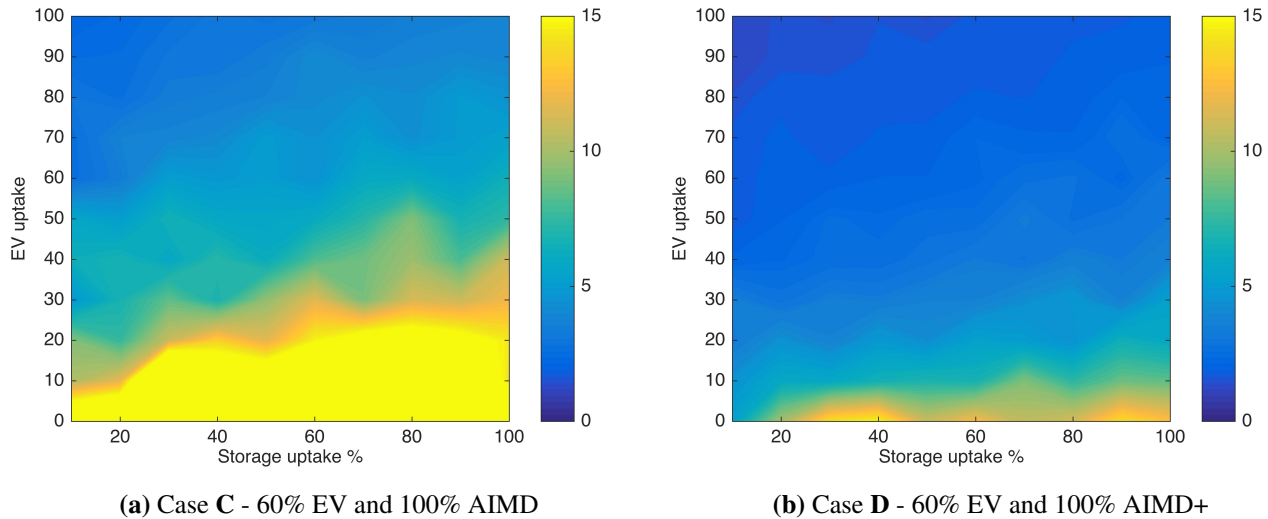


**Figure 15.** Battery power profiles of each load's battery storage device over four days for AIMD (Fig. 15a) and AIMD+ (Fig. 15b).

339

340 This figure shows that for any EV uptake scenario, AIMD controlled energy storage units were cycled  
 341 less equally than the AIMD+ controlled devices. Results show that with a low uptake of EVs, both  
 342 the AIMD and AIMD+ algorithm performed worse, improving as electric vehicle uptake is increased.  
 343 Removing Electric Vehicle uptake from the analysis, the performance difference between AIMD and  
 344 AIMD+ becomes more visible. The resulting averaged  $\zeta_C^{***}$  and  $\zeta_D^{***}$  values for their corresponding  
 345 storage uptake percentages are presented in Figure 16.

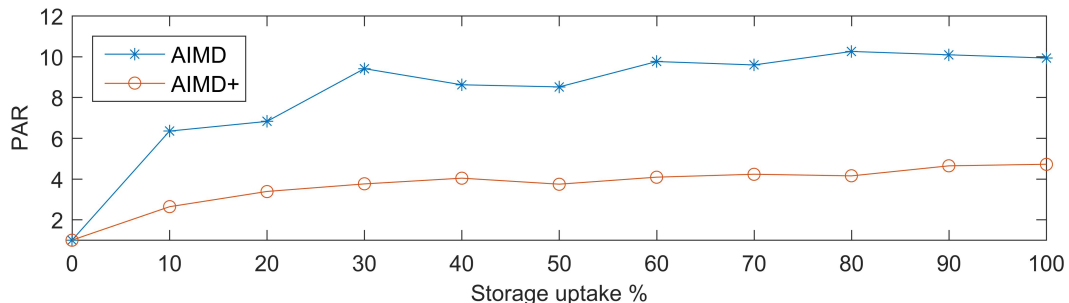


**Figure 16.** The performance index  $\zeta_C^{***}$  for AIMD storage and  $\zeta_D^{***}$  for AIMD+ storage control against storage uptake.

346 Although the AIMD controlled batteries were, on average, cycled less than the batteries controlled by  
 347 the proposed AIMD+ algorithm, just looking at the average produces a distorted understanding of the  
 348 performance. In fact, as more than half of the assigned AIMD energy storage devices never partook in

349 the network control, a lower average cycling is expected. The variation in cycling across all batteries, or  
350 the cycling Peak-to-Average Ratio, reveals the difference between usage and effective usage. The lower  
351 ratio indicating a better usage of the deployed batteries.

## 352 **6. Conclusions**

353 In this paper, a distributed battery energy storage algorithm for mitigation of uncontrolled loads,  
354 such as the charging of Electric Vehicles, is proposed. The proposed AIMD+ algorithm uses local bus  
355 voltage measurements and a reference voltage profile derived from power flow analysis of the distribution  
356 network. The addition of the reference profile takes into consideration the distance of the battery units  
357 to their feeding substation and is used to determine the rate of power increase when charging and  
358 discharging the battery. Simulations were performed on the IEEE European test case and a set of real  
359 UK suburban networks. Comparisons were made of the standard AIMD algorithm with fixed voltage  
360 threshold against the proposed AIMD+ algorithm using a reference voltage threshold. A set of European  
361 demand profiles and realistic electric vehicle travel model were used.

362 For the conducted simulations, the AIMD controlled energy storage performance was improved by  
363 using the computed reference voltage profile. The improved AIMD algorithm resulted in a reduction of  
364 voltage variation and an increased utilisation of available line capacity, which also reduced the frequency  
365 of line overloads. Additionally, the same algorithm equalised cycling and utilisation of battery energy  
366 storage, making most use of the deployed battery assets. To take this work further, future work will  
367 also consider distributed generation, such as photovoltaic panels (PV), beside electric vehicle uptake, as  
368 well as decentralised methods for determining voltage reference values so no prior network knowledge  
369 is required.

## 370 **Acknowledgments**

371 The authors would like to thank SSE-PD for providing the network information for the utilised UK  
372 feeder models.

## 373 **Author Contributions**

374 The two lead authors contributed equally to this piece of work and were supervised by Dr William  
375 Holderbaum and Dr Ben A. Potter.

## 376 **Conflicts of Interest**

377 The authors declare no conflict of interest.

## 378 **References**

- 379 1. Shah, V.; Booream-Phelps, J. F.I.T.T. for Investors: Crossing the Chasm. Technical report, 2015.
- 380 2. Department for Business Enterprise and Regulatory (DBER).; Department for Transport (DfT).  
381 Investigation into the Scope for the Transport Sector to Switch to Electric Vehicles and Plug- in  
382 Hybrid Vehicles. Technical report, 2008.

- 383 3. Ecolane.; University of Aberdeen. Pathways to high penetration of electric vehicles. Technical  
384 report, 2013.
- 385 4. Clement-Nyns, K.; Haesen, E.; Driesen, J. The impact of Charging plug-in hybrid electric  
386 vehicles on a residential distribution grid. *IEEE Trans. Power Syst.* **2010**, *25*, 371–380.
- 387 5. Pieltain Fernández, L.; Gómez San Román, T.; Cossent, R.; Mateo Domingo, C.; Frías, P.  
388 Assessment of the impact of plug-in electric vehicles on distribution networks. *IEEE Trans.*  
389 *Power Syst.* **2011**, *26*, 206–213.
- 390 6. Hadley, S.W.; Tsvetkova, A.a. Potential Impacts of Plug-in Hybrid Electric Vehicles on Regional  
391 Power Generation. *Electr. J.* **2009**, *22*, 56–68.
- 392 7. Putrus, G.; Suwanapongkarl, P.; Johnston, D.; Bentley, E.; Narayana, M. Impact of electric  
393 vehicles on power distribution networks. 2009 IEEE Veh. Power Propuls. Conf., 2009, pp.  
394 827–831.
- 395 8. Pillai, J.R.; Bak-Jensen, B. Vehicle-to-grid systems for frequency regulation in an islanded  
396 Danish distribution network. *2010 IEEE Veh. Power Propuls. Conf. VPPC 2010* **2010**.
- 397 9. Zhou, K.; Cai, L. Randomized PHEV Charging Under Distribution Grid Constraints. *IEEE*  
398 *Trans. Smart Grid* **2014**, *5*, 879–887.
- 399 10. Mohsenian-Rad, A.H.; Wong, V.W.S.; Jatskevich, J.; Schober, R.; Leon-Garcia, A. Autonomous  
400 demand-side management based on game-theoretic energy consumption scheduling for the future  
401 smart grid. *IEEE Trans. Smart Grid* **2010**, *1*, 320–331.
- 402 11. Deilami, S.; Masoum, A.S. Real-time coordination of plug-in electric vehicle charging in smart  
403 grids to minimize power losses and improve voltage profile. *IEEE Trans. Smart Grid* **2011**,  
404 *2*, 456–467.
- 405 12. Masoum, A.S.; Deilami, S.; Member, S.; Masoum, M.A.S.; Member, S. Fuzzy Approach for  
406 Online Coordination of Plug-In Electric Vehicle Charging in Smart Grid. *IEEE Trans. Sustain.*  
407 *Energy* **2015**, *6*, 1112–1121.
- 408 13. Karfopoulos, E.L.; Hatziargyriou, N.D. A Multi-Agent System for Controlled Charging of a  
409 Large Population of Electric Vehicles. *IEEE Trans. Power Syst.* **2013**, *28*, 1196–1204.
- 410 14. Wu, C.; Mohsenian-Rad, H.; Huang, J. Vehicle-to-aggregator interaction game. *IEEE Trans.*  
411 *Smart Grid* **2012**, *3*, 434–442.
- 412 15. Samadi, P.; Mohsenian-Rad, H.; Schober, R.; Wong, V.W.S. Advanced Demand Side  
413 Management for the Future Smart Grid Using Mechanism Design. *IEEE Trans. Smart Grid*  
414 **2012**, *3*, 1170–1180.
- 415 16. Xu, N.Z.; Chung, C.Y. Challenges in Future Competition of Electric Vehicle Charging  
416 Management and Solutions. *IEEE Trans. Smart Grid* **2015**, *6*, 1323–1331.
- 417 17. Chiu, D.M.; Jain, R. Analysis of the increase and decrease algorithms for congestion avoidance  
418 in computer networks, 1989.
- 419 18. Stüdli, S.; Crisostomi, E.; Middleton, R.; Shorten, R. A flexible distributed framework for  
420 realising electric and plug-in hybrid vehicle charging policies. *International Journal of Control*  
421 **2012**, *85*, 1130–1145.
- 422 19. Stüdli, S.; Crisostomi, E.; Middleton, R.; Shorten, R. Optimal real-time distributed V2G and  
423 G2V management of electric vehicles. *Int. J. Control* **2014**, *87*, 1153–1162.

- 424 20. Stüdli, S.; Crisostomi, E.; Middleton, R.; Braslavsky, J.; Shorten, R. Distributed Load  
425 Management Using Additive Increase Multiplicative Decrease Based Techniques. In *Plug Electr.  
426 Veh. Smart Grids*; Springer Singapore, 2015; pp. 173–202.
- 427 21. Mareels, I.; Alpcan, T.; Brazil, M.; de Hoog, J.; Thomas, D.a. A distributed electric vehicle  
428 charging management algorithm using only local measurements. *Innov. Smart Grid Technol.  
429 Conf. (ISGT), 2014 IEEE PES*; , 2014; pp. 1–5.
- 430 22. Munkhammar, J.; Bishop, J.D.; Sarralde, J.J.; Tian, W.; Choudhary, R. Household electricity  
431 use, electric vehicle home-charging and distributed photovoltaic power production in the city of  
432 Westminster. *Energy Build.* **2015**, *86*, 439–448.
- 433 23. Dallinger, D.; Wietschel, M. Grid integration of intermittent renewable energy sources using  
434 price-responsive plug-in electric vehicles. *Renew. Sustain. Energy Rev.* **2012**, *16*, 3370–3382.
- 435 24. Infas.; Deutsches Zentrum für Luft- und Raumfahrt e.V. Mobilität in Deutschland 2008.  
436 Technical report, Bonn und Berlin, Deutschland, 2008.
- 437 25. Rowe, M.; Member, S.; Yunusov, T.; Member, S.; Haben, S.; Singleton, C.; Holderbaum, W.;  
438 Potter, B. A Peak Reduction Scheduling Algorithm for Storage Devices on the Low Voltage  
439 Network. *IEEE Trans. Smart Grid* **2014**, *5*, 2115–2124.
- 440 26. Laresgoiti, I.; Käbitz, S.; Ecker, M.; Sauer, D.U. Modeling mechanical degradation in lithium  
441 ion batteries during cycling: Solid electrolyte interphase fracture. *J. Power Sources* **2015**,  
442 *300*, 112–122.
- 443 27. UK Government Digital Service. Vehicle free-flow speeds (SPE01), 2013.
- 444 28. Rowe, M.; Yunusov, T.; Haben, S.; Holderbaum, W.; Potter, B. The real-time optimisation  
445 of DNO owned storage devices on the LV network for peak reduction. *Energies* **2014**,  
446 *7*, 3537–3560.
- 447 29. Society, I.P.; Energy. European Low Voltage Test Feeder, 2015.
- 448 30. Thames Valley Vision. <http://www.thamesvalleyvision.co.uk>. Accessed: 2016-01-27.
- 449 31. Papaioannou, I.T.; Purvins, A.; Demoulias, C.S. Reactive power consumption in photovoltaic  
450 inverters: a novel configuration for voltage regulation in low-voltage radial feeders with no need  
451 for central control. *Progress in Photovoltaics: Research and Applications* **2015**, *23*, 611–619.

452 © January 30, 2016 by the authors; submitted to *Energies* for possible open access  
453 publication under the terms and conditions of the Creative Commons Attribution license  
454 <http://creativecommons.org/licenses/by/4.0/>.